THE MODIFICATIONS OF NEAR-WALL TURBULENCE STRUCTURE AND HEAT TRANSFER BY IMMISCIBLE DROPLETS IN TURBULENT LIQUID-LIQUID TWO-PHASE FLOW

Takuji Yuge, Yoshimichi Hagiwara
Department of Mechanical and System Engineering
Kyoto Institute of Technology,
Matsugasaki, Kyoto 606-8585, Japan
yuge02@ipc.kit.ac.jp, yoshi@ipc.kit.ac.jp

ABSTRACT

Direct numerical simulation has been carried out for non-isothermal turbulent upward channel flow with four immiscible droplets whose density is higher than that of continuous-phase flow. The interface was tracked by the modified volume-of-fluid method. The computational results show that both the outward flow in the wake and the wallward flow around the cap of a droplet enhance heat transfer. These flows are attenuated by the adjacent droplet in the axial direction. The droplets prevent the evolution of hairpin vortices and attenuate the developed vortices.

INTRODUCTION

Flow characteristics and heat transfer of turbulent liquid flow with immiscible droplets have been the focus of recent research. It is crucial to elucidate this phenomenon for developing a liquid-liquid direct-contact heat exchanger. This new heat exchanger provides one of the most effective equipments for recovery of exhaust heat in warm water from buildings and factories with temperature close to the ambient in order to use energy efficiently and protect environment (Kadoguchi, 2002). Lee (1987) measured the droplet size distribution and the overall heat transfer coefficient in the direct-contact process. Kaviany (1994) investigated the interaction between a droplet and its surrounding flow. Inaba et al. (1998) obtained empirical equations for the size distribution of droplets injected into water flow and inter-phase heat transfer. These results all provide useful data for designing the heat exchanger.

However, the effect of a wall on the flow characteristics and heat transfer of the dispersed liquid-liquid two-phase flow was not considered in these studies. This is because the droplets are located far from the wall in these studies. To consider the effect is crucial for developing a small-scale heat exchanger. The present authors concluded from their simulation that the outward component of the wake flow of a counter-moving droplet induces the liftup of the fluid with high temperature adjacent to the heating wall in turbulent downward flow (Hagiwara et al., 2003a) or upward flow (Hagiwara et al., 2003b). We also showed that the wallward component of the impinging flow on the rising droplet cap brings low-temperature fluid into the near-wall region in each case. Only one droplet was considered in these studies. Therefore, the effects of another droplet in the neighborhood on the numerical results were not discussed.

In the present numerical study, we carry out a direct numerical simulation of turbulent heat transfer in upward channel flow with four droplets of high density. We consider water for the continuous phase fluid and hydrofluoroether for the dispersed phase fluid. This liquid has the advantage of both low global warming potential and zero ozone-depletion potential. We focus on the interaction between near-wall turbulence structures and the droplets and heat transfer associated with the interaction are discussed.

COMPUTATIONAL DOMAIN AND SCHEMES

The computational domain was a rectangular box in a turbulent flow between two vertical walls at the distance of $2h$. The origin of the coordinate was set at a bottom corner of the domain. The x, y and z axes were positioned in the streamwise, wall-normal and transverse directions, respectively. The domain size was $8h \times 2h \times 4h$.

The domain was divided into $128 \times 100 \times 128$ rectangular cells of volume of $\Delta V = \Delta x \times \Delta y(y) \times \Delta z$. Δx and Δz ($=\Delta x/2$) were unchanged, while $\Delta y(y)$ was taken as $\Delta y(y) = \Delta z$ for $0.25 \le y/h \le 1.75$, $\Delta y(y) = \Delta z/2$ for $0.125 \le y/h \le 0.25$ and $1.75 \le y/h \le 1.875$, $\Delta y(y) = \Delta z/4$ for $0.016 \le y/h \le 0.125$ and $1.875 \le y/h \le 1.984$, and $\Delta y(y) = \Delta z/8$ for $0 \le y/h \le 0.016$ and $1.984 \le y/h \le 2$. These dimensions are suitable for grid refinement as mentioned below. The Reynolds number, Re_τ, based on the friction velocity, u_τ, was 180.

In Table 1, the domain size, the grid spacing and the Reynolds numbers are compared with those adopted in direct numerical simulations for channel flows without droplets carried out by Kuroda and Kasagi (1992) with a spectral method and Kawamura et al. (1998) with a finite difference scheme.

Table 1 : Comparison of domain size and grid spacing

	$L_x \times L_z$	$\Delta x^+ \times \Delta y^+ (y) \times \Delta z^+$	Re_τ
Kuroda	$12.8h \times 6.4h$	$18 \times$ NA $\times$ 9	180
Kawamura	$6.4h \times 3.2h$	$9 \times 0.40\text{-}11.5 \times 4.5$	180
Present	$8h \times 4h$	$11.3 \times 0.70\text{-}5.6 \times 5.6$	180

COMPUTATIONAL SCHEMES

The computational schemes adopted in the present study are the same as those in our previous studies (Iwasaki, et al., 2001; Hagiwara et al., 2003a; Hagiwara et al., 2003b): The NS equations and the energy equations were solved by using the finite difference schemes of the staggered type and the fractional-step method. The second-order central difference scheme based on the interpolation method and the second-order central difference scheme were applied for the finite-differencing of the convection and the viscous terms, respectively. The temperature was defined at the same location of the wall-normal velocity. Poisson's equation for the pressure field was solved directly by using Fast Fourier Transforms and Gaussian elimination methods. The third-order Runge-Kutta method was used for the time-integration of the convective, viscous, and forcing terms in NS equations and the diffusion terms of energy equations.

In the wall-normal direction, the non-slip boundary condition was imposed for velocity components. Similarly, the Neumann boundary condition was given for the pressure. The constant wall temperature and the constant wall hat flux were assumed. The periodical boundary conditions were given for all the variables in the streamwise and transverse directions. The Prandtl number was set equal to 2.0.

MODIFIED VOF ALGORITHM

The position of the interface was determined by the fraction of the continuous-phase fluid, F, occupying a cell. F=1 represents a cell filled with the continuous-phase fluid, while F=0 indicates that the cell is filled with the fluid of the droplet. The cells of $0 < F < 1$ include the interface. The time evolution of F was estimated with the modified Volume of Fluid (VOF) algorithm (Hirt and Nichols, 1981). We classified the intersection of the interface to the surfaces of the cubic cell (figure omitted). In the case when the interface intersected two parallel surfaces of the cell, the value of F was determined by the Donor-Accepter method. We took account of the slope of the interface in this method. In the other cases, we solved the following convection equation

$$\frac{\partial F}{\partial t} = -u\frac{\partial F}{\partial x} - v\frac{\partial F}{\partial y} - w\frac{\partial F}{\partial z}. \qquad (1)$$

In order to obtain more points near the interface and to approximate the interface more locally and precisely, the local grid refinement (Tanaka et al., 1997) was adopted. In this technique, each original cell near the interface is further divided into fine cubic cells of sides $\Delta\tilde{x} = \Delta x/8$ (See Fig. 1). The points on the interface were calculated for fine cells which contain the interface by using the values of F. Equation (1) was discretised on these fine grids. The values of the velocity components at the fine grids, required for solving Eq. (1), were estimated firstly by linear interpolation of the velocity components of the original cells, and then the estimated velocity was corrected so that the equation of continuity was satisfied for each fine cell at every time step. The local grid refinement was also effective for reducing the numerical diffusion of F.

VISCOUS COEFFICIENT

In order to evaluate the viscous term in the NS equations, the value of the viscous coefficient is needed at the volume center ($\boldsymbol{x}_a$) or the centers of the sides ($\boldsymbol{x}_b$) of the cell, depending on the special derivatives. It was evaluated as

$$\mu(x) = \overline{F}(x)\cdot\mu_c + \left(1 - \overline{F}(x)\right)\cdot\mu_d \qquad (2)$$

where μ_c and μ_d are the viscous coefficients for the continuous and dispersed phases respectively and fluid $\overline{F}$ is the average of F over the domain whose dimension is the same as the original cell and whose center is located at $\boldsymbol{x} = \boldsymbol{x}_1$ or $\boldsymbol{x}_2$ (the box drawn by the solid lines and that by the broken lines in Fig. 2, respectively). The evaluation of the viscous coefficient near the interface gives high accuracy for the calculation of the viscous term.

INTERFACIAL TENSION

The interfacial tension was calculated by the following procedure. Let N_m (m=1, 2, $\cdots M$) being the points of intersections between the spherical surface, which approximates the interface and the sides of the original cell (See Fig. 3). Here, the unit vector normal to the interface, $\boldsymbol{n}$, was estimated as

$$\boldsymbol{n} = \sum_{m=1}^{M} \boldsymbol{n}_m \Big/ \left| \sum_{m=1}^{M} \boldsymbol{n}_m \right|$$

where $\boldsymbol{n}_m = \overrightarrow{CN_m}$ (m=1, 2, $\cdots M$) and C denotes the center of the sphere. The area of the spherical surface, S, was approximated by the sum of those of triangles which consist of the points N_m (m=1, 2, $\cdots$ M), and the point of intersection between the spherical surface and the normal vector.

Using S and the radius R of the sphere obtained above, the external body force in NS equations was calculated as

$$f\cdot\Delta V = \sigma(1/R_1 + 1/R_1)S(-\boldsymbol{n}) = \sigma(2/R)S(-\boldsymbol{n}), \qquad (3)$$

where σ is the coefficient of the interfacial tension.

Table 2: Physical properties

	Present computation	Hydrofluoro-ether
Interfacial tension σ^+	2160	9100
Density ratio ρ_d/ρ_c	1.43	1.43
Viscosity ratio μ_d/μ_c	30	0.65
Specific-heat ratio Cp_d/Cp_c	0.29	0.29
Prandtl-no. ratio Pr_d/Pr_c	1	1.66

COMPUTATIONAL CONDITION FOR DROPLETS

We introduced four identical droplets with diameters of $6\Delta x$ ($=48\,\Delta\tilde{x}=67.5\nu/u_\tau$) into near-wall region. At the initial state, the centers of all the droplets were allocated at the vertices of a square whose one-side length was 154 wall units and distance from one wall was 73 wall units. The computational condition for the droplet properties are compared with those of hydrofluoroether droplet in Table 2.

RESULTS AND DISCUSSION

Turbulence statistics

The turbulence statistics were calculated for a period of $1800\nu/u_\tau^2$ before the initial field of velocity and temperature was obtained. Figure 4 shows the mean velocity profile. Figure 5 indicates the profiles of turbulence intensities in the streamwise, wall-normal and transverse directions. Figure 6 depicts the profiles of the viscous shear stress, $\mu\left(d\bar{u}/dy\right)$, the Reynolds shear stress, and the sum of these stresses. The DNS results of the spectral method obtained by Kuroda and Kasagi (1992) is also indicated by the broken lines in these figures. Our computational results are in agreement with those of the spectral method.

Figures 7 and 8 show the profiles of the mean temperature and the root-mean-square values of temperature fluctuation. These mean and rms values are in the nondimensional form by using the friction temperature, θ_τ $[=q_w/(\rho Cpu_\tau)]$. Since the DNS results for the channel flow heat transfer in the case of Pr=2 are not available, our results in the case of Pr=1.5 are compared with those obtained by Kawamara et al. (1998). Our result for Pr=1.5 is in agreement with that of Kawamura. The fact that our result for Pr=2.0 takes higher values than that for Pr=1.5 is consistent with the results of Pr=1.5 and Pr=1 obtained by Kawamura. Thus, the computational methods used for the continuous-phase flow is verified from these results.

Secondary flow around droplets

We discuss the interaction between main flow and droplets for a short period by using some snapshots in this and the next section.

Figure 9 demonstrates the velocity fluctuation and the gray-scale contour map of temperature on the (x, y)-plane including the centers of the droplets on the right-hand-side. The bold curve shows the interface. The white area indicates a lower temperature region, while the black area indicates a higher temperature region.

Noticeable velocity vectors due to the gravitational force are seen inside and below the droplets. The velocity of the upper droplet is slightly higher than that of the lower velocity. This is because the upper droplet is inside the wake flow region of lower droplet where the impinging main flow is decelerated by the lower droplet. Similar reaction of the upper droplet to the lower droplet was observed in our recent measurement (Tajima, 2003). The Reynolds numbers based on the relative velocities and the droplet diameters were in the range of 450-680. Their mean value is approximately equal to that measured for the hydrofluoroether droplets (Tajima, 2003).

The secondary flow is seen on both sides of the droplets. Noticeable upward secondary flow is seen between the lower droplet and the wall. The flow is accelerated in this region. The secondary flow in this region resembles a wall jet. Part of this jet-like flow changes direction to the outward and approaches the right bottom of the upper droplet. The downward velocity vectors of the upper droplet changes the direction by the jet-like flow. At the same time, the flow along the left-hand-side of the upper droplet becomes predominant. The upper droplet is found to move outward after this moment. Thus, the wake flow of the lower droplet affects directly the secondary flow and the motion of the upper droplet in the case of short distance between the droplets. This cannot be predicted by the previous simulation for a droplet. It should be noted that the similar motion of hydrofluoroether droplet with flow along the interface of facing away from the wall was observed in our previous measurement (Hagiwara, et al., 2003b).

The other part of the wall-jet-like flow passes through the gap between the wall and the upper droplet. Therefore, high-speed upward flow is seen in a wide region adjacent to the wall near the droplets. A large-scale hairpin vortex, which is seen near the middle part of the opposite wall, is not observed in this region.

Figure 10 shows velocity vectors and the gray-scale contour of temperature on a cross-sectional (y, z)-plane below the cap of the lower droplets in the impinging flow region. Large-scale circulating motions are seen near the upper wall. These are the streamwise legs of two hairpin vortices identified by the method proposed by Jeong and Hussain (1995). Similar large-scale motion is not seen near the lower wall except in the lower-left region of the left-hand-side droplet where the developed hairpin vortex interacts with the droplet. Therefore, the near-wall droplets disturb the development of hairpin vortices.

It is found that the impinging flow diverges 360 degrees at the caps of the droplets. The highest value for the ratio of the Reynolds-shear stress product to the local Reynolds shear stress, $-uv/\left(-\bar{u}\bar{v}(y)\right)$, around the cap of the droplet was 1.2-8.1 times higher than that in the case without the droplets.

Figure 11 indicates velocity vectors and the gray-scale contour of temperature on a (y, z)-plane above the tail of the lower droplets in their wake regions. The droplet has already passed through the plane from above and is leaving from the plane. The broken lines show the projection of lower droplets. The flows from the wall to the wake region are observed. The flow for the left-hand-side droplet interacts strongly with the hairpin vortex, and part of the flow is involved in the vortex.

Figure 12 depicts velocity vectors and the gray-scale contour of temperature on a (y, z)-plane below the cap of the upper droplets in the impinging flow region. This figure is similar to Fig. 10 except for the upward flow above the right-hand-side droplet and flows along the interface and in the left direction for the left-hand-side droplet. The upward flow is associated with the secondary flow along the interface facing away from the wall shown in Fig. 9. The flow around the right-hand-side droplet is the result of modification and attenuation of the hairpin vortex by the droplet.

Figure 13 demonstrates velocity vectors and the gray-scale contour of temperature on a cross-sectional (y, z)-plane above the tail of the upper droplets in their wake regions. The droplet has already passed through the plane from above and is

leaving from the plane. The broken lines show the projection of the upper droplets. A pair of counter-rotating fluid motion is observed between the right-hand-side droplet and the wall. This is due to the newly generated vortices from the interface. Similar vortices were predicted at the same location of interface for immiscible droplet (Iwasaki et al., 2001) A gathering flow from the central region to the center of the wake flow region. This is caused by the secondary flow along the interface of facing away from the wall. A similar flow was observed and predicted in our previous study for an isolated descending droplet in upward flow (Hagiwara et al., 2003b).

Modification of heat transfer mechanism by droplets

In Fig. 9, a high temperature region (gray) is found to spread between the high-speed upward flow and the wall-jet-like flow impinging on the upper droplet. The wall-jet-like flow in the outward direction transports fluid lumps with high temperature in this region. The high-speed upward flow also contributes to the convective heat transfer in the streamwise direction. Thus, the turbulent heat transfer mechanism is different from that without the influence of the droplet.

In Fig. 10, the spread of high-temperature regions (dark gray) in the outward direction due to the ejection associated with the vortices is observed only in the region farthest away from the droplets. The wallward intrusion of low-temperature regions (light gray or white) due to the sweep associated with the vortices is also observed in these regions. Therefore, the near-wall droplets disturb the development of hairpin vortices.

On the other hand, the wallward component of the flow along the cap in Fig. 10 brings low-temperature fluid into the near-wall region. In particular, the high-temperature regions are very thin at the passage between the right-hand-side droplet and the wall. The highest value for the ratio of the product of wall-normal velocity fluctuation and the temperature fluctuation to the local turbulent heat flux $v\theta/\overline{v\theta}$ around the cap of the droplet was 2.1-6.6 times higher than that in the case without droplets. Therefore, the secondary flows associated with the droplets are found to be effective for the enhancement of the near-wall heat transfer.

The liftup of high-temperature fluid from the wall to the right-hand-side droplet is clearly seen in Figs. 11 and 13. This corresponds to the high temperature region caused by the wall-jet-like flow mentioned above. Low-temperature fluid flows into this region from both sides. This enhances heat transfer.

In Fig. 12, the high-temperature region adjacent to the wall become thinner compared with that seen in Fig. 10. This is due to the high-speed upward flow along the wall mentioned above. The low temperature regions induced by the impinging flow is not noticeably because the flow is not as strong when compared with the lower droplet. The liftup of hot fluid by the ejection was attenuated due to the damage of the hairpin vortex by the right-hand-side droplet.

Conceptual model of droplet/flow interaction

Figure 14 shows conceptual model of the interaction. The secondary flows generally enhance the momentum and heat transfer, while the damage to the hairpin vortices causes the attenuation of heat transfer.

CONCLUSIONS

The direct numerical simulation was carried out for a turbulent upward flow between two heating walls with four immiscible droplets. The interface was tracked by the modified VOF algorithm. The main conclusions obtained are as follows.

1. The droplet induced several types of secondary flows. These flows increased the Reynolds shear stress product. These flows were attenuated by the adjacent droplet in the streamwise direction.
2. The hairpin vortices were not evolved near the droplets. The developed hairpin vortices were deformed by the droplet. The vortices modified the secondary flows.
3. The product of wall-normal velocity fluctuation and the temperature fluctuation increased by the secondary flows. This shows an enhancement of turbulent heat transfer by the droplets.

Acknowledgements

This study was supported by the Japan Society for Promotion of Science through the Grant-in-Aid for Scientific Research (No. 14550181).

REFERENCES

Hagiwara, Y., at al., 2003a, "Effects of a droplet on near-wall transport phenomena in turbulent downward liquid-liquid flow", *J. Enhanced Heat Transfer* (to appear).

Hagiwara, Y., at al., 2003b, "Interaction between near-wall turbulence structure and immiscible droplets falling with wobbling motion in upward water flow", *J. Energy* (to appear).

Hirt, C. W., and Nichois, B. D., 1981, "Volume of fluid method for the dynamics of free boundaries", *J. Computational Phys.*, Vol. 39, pp.201-225.

Inaba, H., et al., 1998, "Liquid-liquid direct contact heat exchange using a perfluorocarbon liquid for waste heat recovery" (in Japanese). *Trans. JSME.* Vol. 64B, pp.3838-3845.

Iwasaki, T., et al., 2001, "Direct numerical simulation of turbulent Couette flow with immiscible droplets", *Int. J. Heat and Fluid Flow*, Vol. 22, pp.332-342.

Jeong, J. and Hussain, F., "On the identification of a vortex", *J. of Fluid Mechanics*, Vol.285, 69-94, 1995.

Kadoguchi, K., 2002, "Direct-contact boiling phenomena in a field with the continuous liquid-liquid interface", *Progress in Transport Phenomena*, pp.285-289.

Kaviany, M. *Principles of Convective Heat Transfer*, 1994, Springer-Verlag, New York.

Kawamura, H. et al., 1998, "DNS of turbulent heat transfer in channel flow with low to medium-high Prandtl number fluid", *Int. J. Heat and Fluid Flow*, Vol. 19, pp.482-491.

Kuroda, A. and Kasagi, N., 1992, http://www.thtlab.t.u-tokyo.ac.jp/index/html.

Lee, J. M., 1987, "Drop size formations in agitating system", *Encyclopedia of Fluid Mechanics* (ed. by N. P. Cheremisinoff), Vol. 6, 141-165.

Tajima, M., MS Thesis, Kyoto Institute of Tech., 2003.

Tanaka, M., et al., 1997, "Evaluation in interaction between an immiscible droplet and a liquid laminar Couette flow using local mesh refinement", ISAC'97 High Performance Computing on Multiphase Flows, pp.31-34.

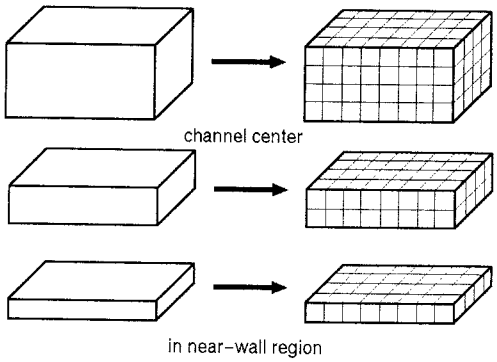

Fig. 1 Local grid refinement

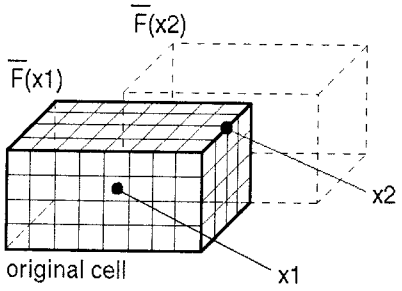

Fig. 2 Boxes and points for evaluation of vicosity

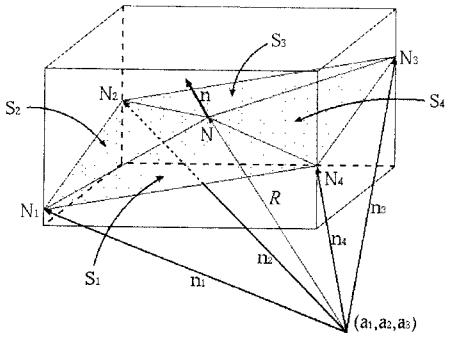

Fig. 3 Estimation of interfacial area and curvature

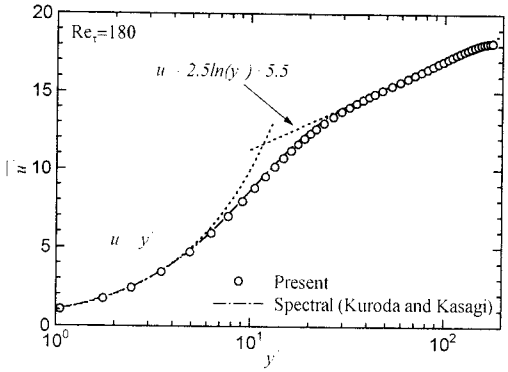

Fig. 4 Mean velocity profile

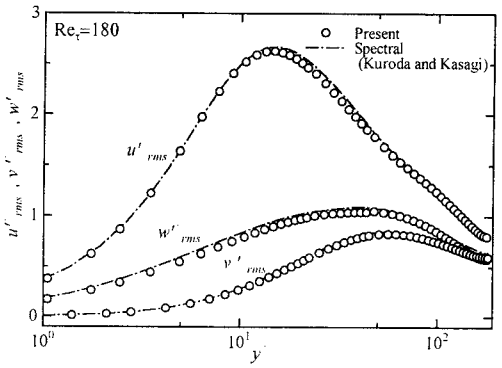

Fig. 5 Turbulence intensities

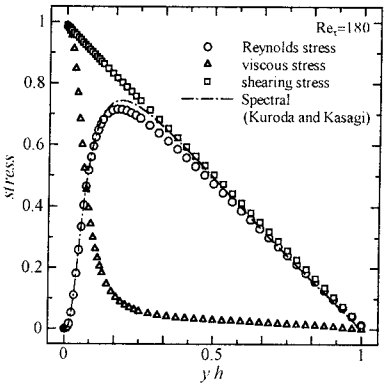

Fig. 6 Stresses

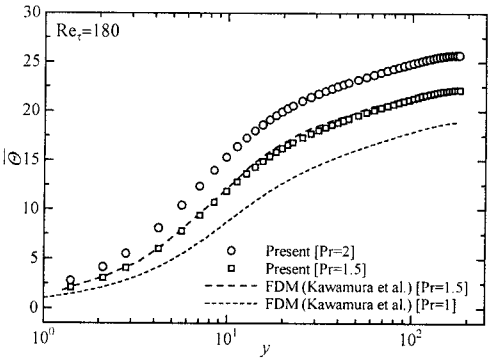

Fig. 7 Mean temperature prifile

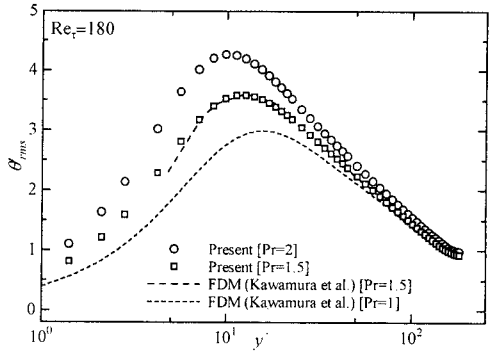

Fig. 8 Root-mean-square of temperature fluctuation

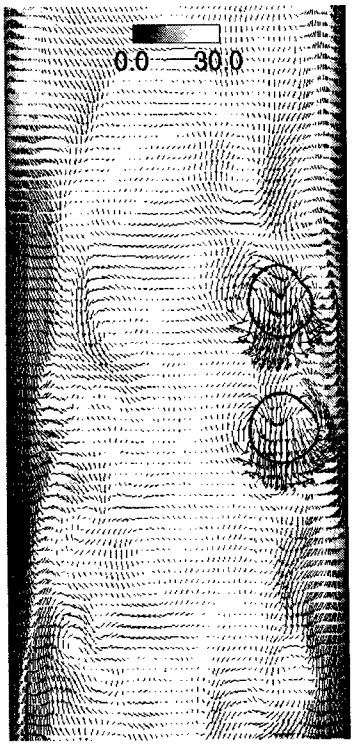

Fig. 9 Velocity fluctuation and contour map of temperature in a (x, y)-plane

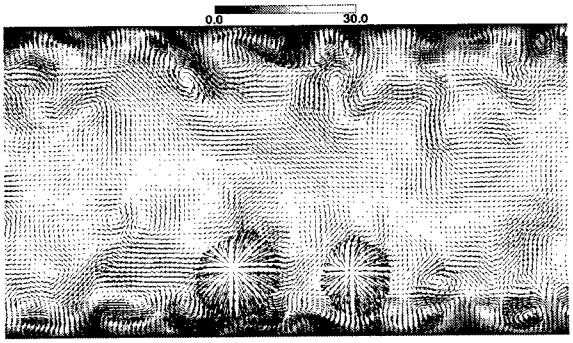

Fig. 10 Velocity fluctuation and contour map of temperature in a (y, z)-plane below the cap of lower droplets

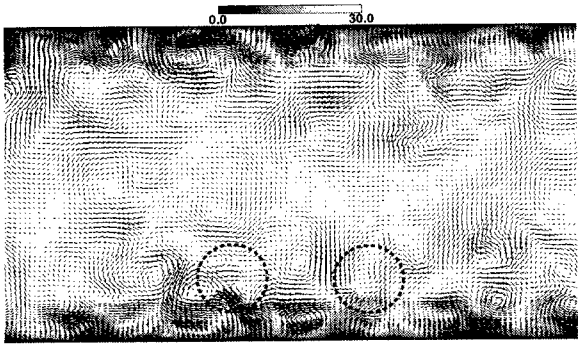

Fig. 11 Velocity fluctuation and contour map of temperature in a (y, z)-plane above the tail of lower droplets

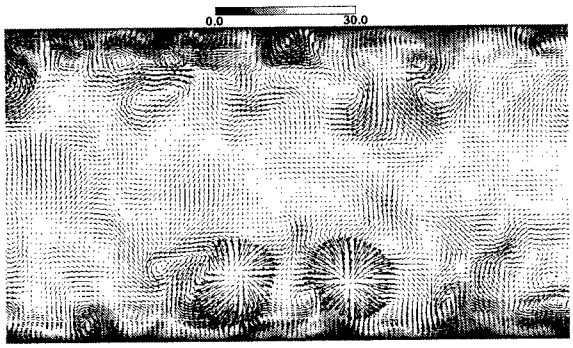

Fig. 12 Velocity fluctuation and contour map of temperature in a (y, z)-plane below the cap of upper droplets

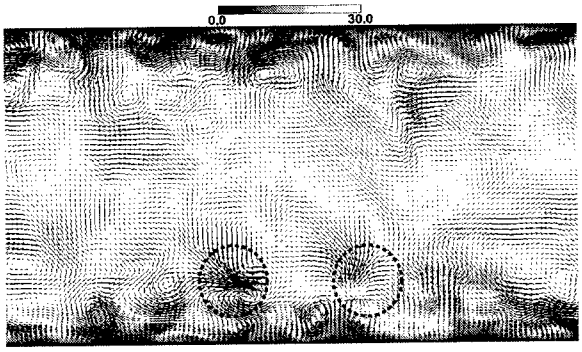

Fig. 13 Velocity fluctuation and contour map of temperature in a (y, z)-plane above the tail of upper droplets

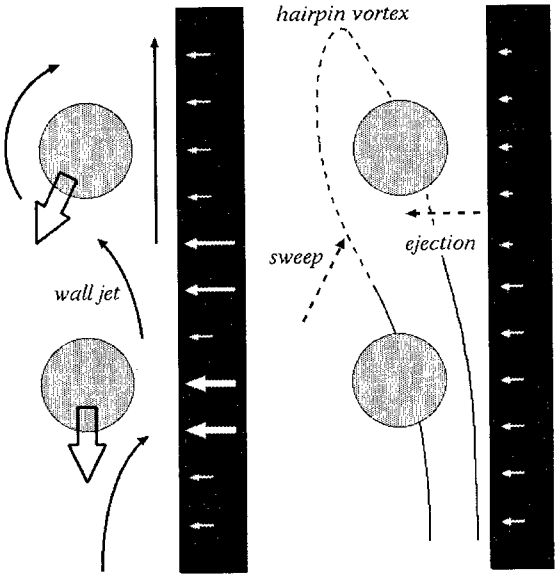

Fig. 14 Conceptual model of secondary flows, attenuation of vortices and modification of heat transfer mechanism